

A new fuzzy clustering algorithm for the segmentation of brain tumor

V. P. Ananthi¹ · P. Balasubramaniam¹ · T. Kalaiselvi²

© Springer-Verlag Berlin Heidelberg 2015

Abstract This paper introduces a new method of clustering algorithm based on interval-valued intuitionistic fuzzy sets (IVIFSs) generated from intuitionistic fuzzy sets to analyze tumor in magnetic resonance (MR) images by reducing time complexity and errors. Based on fuzzy clustering, during the segmentation process one can consider numerous cases of uncertainty involving in membership function, distance measure, fuzzifier, and so on. Due to poor illumination of medical images, uncertainty emerges in their gray levels. This paper concentrates on uncertainty in the allotment of values to the membership function of the uncertain pixels. Proposed method initially pre-processes the brain MR images to remove noise, standardize intensity, and extract brain region. Subsequently IVIFSs are constructed to utilize in the clustering algorithm. Results are compared with the segmented images obtained using histogram thresholding, k-means, fuzzy c-means, intuitionistic fuzzy c-means, and interval type-2 fuzzy c-means algorithms and it has been proven that the proposed method is more effective.

Keywords Brain MR image · Segmentation · Interval-valued intuitionistic fuzzy set · Brain tumor · Clustering

Communicated by V. Loia.

✉ P. Balasubramaniam
balugru@gmail.com

¹ Department of Mathematics, Gandhigram Rural Institute - Deemed University, Gandhigram, Dindigul, Tamil Nadu, India

² Department of Computer Science and Applications, Gandhigram Rural Institute - Deemed University, Gandhigram, Tamil Nadu 624 302, India

1 Introduction

Brain tumor is a region having a mass of abnormal tissues in the brain and is categorized as benign and malignant tumors according to their growth. Benign tumors are slow growing and do not disseminate to their neighboring tissues, but malignant tumor grows aggressively and spreads quickly in the nearby areas.

Magnetic resonance imaging (MRI) is one of the most common brain imaging techniques. Some other imaging techniques are also available such as computed tomography (CT), positron emission tomography (PET). CT provides the hard tissues like bones and MRI renders only soft tissues of the imaging organ but is more efficient than CT because of its contrast.

Treatment for the brain tumor relies on the ability of the physician to identify the position, size, character, and edges of the tumor. The direct analysis provided by the radiologist to the physician furnishes less accurate results due to various limitations like existence of noises in the images and the pattern of human races. In recent decades, computer is used as an aid for locating such tumors through the process of image segmentation.

Segmentation is a basic building block in image analysis. It is a process of dividing an image into significant regions. There are numerous techniques available for image segmentation, namely gray level thresholding, edge detection, histogram thresholding, texture, clustering algorithm (Huang et al. 2015; Li and Shen 2010), region, segmentation based on fractals, wavelets (Farias et al. 2010), and so on. Clustering technique is generally employed in the fields such as image processing, data mining, pattern recognition, and so on. Most of the algorithms in image processing are prone to several uncertainties, for example, grayness ambiguity (uncertainty in the input information itself). The main

aim of this work is to reduce uncertainty while clustering images using powerful uncertainty absorbent.

Zadeh (1965) initiated the concept of fuzzy sets (FSs) in 1965. Later in 1986, Atanassov (1986) introduced intuitionistic fuzzy sets (IFSs) as a generalization of FSs by adding a new parameter called hesitation degree. It is not suitable to use an IFS which has a constant degree of membership and non-membership function for all the time but a range of values vary within an interval, see Bustince et al. (2009). This leads to the innovation of a new fuzzy set with its membership function defined as an interval to detect edges. It is utilized in a number of various domains such as medicine, data processing, and mining. Atanassov and Gargov (1989) generalized IFS by defining membership and non-membership function as an interval value instead of an exact number. Nowadays, the extended FSs such as interval-valued fuzzy set (IVFS), IFS, and interval-valued intuitionistic fuzzy set (IVIFS) are utilized in a great extent to handle the problem of uncertain data, see Bustince et al. (2009), Chaira (2014), Ji et al. (2014), and references therein.

There are two main strategies in clustering technique namely crisp and fuzzy clustering technique. Due to various situations, for images, issues like small scale of spatial resolution, poor illumination, presence of noise, intensity imbrication leads crisp segmentation a hard task. Among numerous clustering techniques, fuzzy c-means (FCM) (Zhou and Zhou 2014) algorithm is more significant because of its robustness. Although it is robust it works only on the images without noise. In order to overcome these drawbacks, the image is pre-processed before commencing the clustering process. Skull stripping is one of the pre-processing step concerned with brain images. Brain extraction is a pre-processing intracranial segmentation in which brain tissue is segmented from skull and non-brain tissue region in MR brain images (Galdames et al. 2012). Performance of tumor extraction methods also depends upon the intensity and contrast of the image, which is influenced mainly by image intensity inhomogeneity (Hou 2006). Standardization of global intensity scale to a local intensity scale is necessary for further segmentation process (Zhung and Udupa 2009). Many researchers have analyzed brain MRI segmentation using FSs, see Zhao et al. (2013), Agrawal et al. (2014). But these algorithms still have problems due to various situations, for example, capturing brain images under poor illumination make it uncertain. After the introduction of IFS, Chaira (2011) showed that IFSs have the ability to remove much uncertainty than FSs by introducing a novel intuitionistic fuzzy c-means (IFCM) clustering algorithm. Bustince and Burillo (1995) have initiated the way for building IVIFS from IFS in a theoretical point of view and fail to explain about the type of uncertainty and how it can be modeled for applications. But in 2010, Xu and Wu (2010) have extended FCM algorithm for clustering IVIFSs and they illustrated with various datasets.

These existing methods have not dealt with proper uncertainty regarding their source dataset. To overcome the issue, in the proposed method uncertainty is considered according to its source dataset.

This paper concerns with the segmentation of brain tumors in brain MR images using new c-means algorithm based on IVIFS. Initially, images are enhanced using median filter to reduce noise and brain is extracted using the skull stripping method. Then IVIFS for the enhanced brain MR image is generated from the IFS, which is obtained from an FS. Then IVIFS is clustered by utilizing the proposed interval-valued intuitionistic fuzzy c-means (IVIFCM) clustering algorithm. Experimental results are provided to render the performance of the proposed algorithm and are compared with thresholding (HT), k-means (KM), FCM, IFCM, and interval type-2 fuzzy c-means (ITFCM) clustering algorithms. Quantitative performance of the proposed algorithm is found by calculating Dice coefficient of the clustered results to show the accuracy of the segmentation process. Area of the tumors is calculated from the clustered outputs, which helps the physician to find the severeness of the tumor and the way to treat that particular person.

This paper is framed as follows. Section 2 explains some basic concepts of FSs, IFSs, and IVIFSs. In Sect. 3, IVIFS is constructed from IFS. Steps of the IVIFCM clustering algorithm along with some pre-processing works are drawn in Sect. 4. Section 5 describes briefly about the performance metrics utilized for quantitative analysis of the algorithm. Experimental results are discussed in Sect. 6. Finally, the conclusion is depicted in Sect. 7.

2 Basic concepts of FSs and their extensions

This section explains roughly about FSs and their extensions such as IFSs and IVIFSs.

2.1 Fuzzy sets (FSs)

Let $X = \{x_1, x_2, \dots, x_n\}$ be a non-empty finite set. A fuzzy set (Zadeh 1965) F of X can be defined as

$$F = \{(x, \mu_F(x)) | x \in X\},$$

where $\mu_F(x) : X \rightarrow [0, 1]$ expresses the degree of belongingness of x in X and the degree of non-belongingness of x in X can be simply obtained using the equation $1 - \mu_F(x)$.

2.2 Intuitionistic fuzzy sets (IFSs)

An IFS F in X can be formulated as

$$F = \{(x, \mu_F(x), \nu_F(x)) | x \in X\},$$

where $\mu_F(x), \nu_F(x) : X \rightarrow [0, 1]$ represent the degree of belongingness and non-belongingness of x in X , respectively, with the essential condition $0 \leq \mu_F(x) + \nu_F(x) \leq 1$.

As this paper concerns with segmentation of tumors in uncertain brain MR image, so there arises hesitation in determining the membership function of the uncertain pixel due to lack of knowledge. For this reason, [Atanassov \(1986\)](#) proposed an IFS having a third parameter called hesitation degree which is then utilized for eliminating uncertainty and is calculated as $\pi_F(x) = 1 - \mu_F(x) - \nu_F(x)$, further the equality $\mu_F(x) + \nu_F(x) + \pi_F(x) = 1$ holds for all $x \in X$. Hence, IFS F in X can be reformulated as

$$F = \{ \langle x, \mu_F(x), \nu_F(x), \pi_F(x) \rangle | x \in X \}.$$

2.3 Interval-valued intuitionistic fuzzy sets (IVIFSs)

An IVIFS \tilde{F} over X is mathematically formulated as

$$\tilde{F} = \{ \langle x, M_{\tilde{F}}(x), N_{\tilde{F}}(x) \rangle | x \in X \},$$

where $M_{\tilde{F}}(x)$ and $N_{\tilde{F}}(x) \subset [0, 1]$ are membership and non-membership intervals, respectively, and $\sup M_{\tilde{F}}(x) + \sup N_{\tilde{F}}(x) \leq 1$, for all $x \in X$.

3 Construction of IVIFS for the brain MR image

This section constructs an IVIFS from an IFS which is generated from a FS.

3.1 Generating IFS from FS

The source images are initially fuzzified. Then what is fuzzy in the brain MR images will become an immediate question. In general, most of the medical images are not properly illuminated, which lead pixel uncertainty related to the levels of brightness and is considered as fuzzy throughout this paper. Clearly, fuzzy domain is a subset of a spatial domain. So, membership function of gray level is utilized directly by optimizing normalized gray level of the particular brain MR image.

The brain MR image I of $S \times T$ dimension is considered as an array of fuzzy singletons. A fuzzy singleton is a FS whose support is a single point where the support of a FS F in X is defined as $Supp(F) = \{x \in X | \mu_F(x) > 0\}$.

The brain MR image I is fuzzified using the following equation:

$$\mu_I(I(i, j)) = \frac{gl - gl_{\min}}{gl_{\max} - gl_{\min}}, \tag{1}$$

where gl is the intensity value of (i, j) th pixel, and gl_{\max} and gl_{\min} denote the highest and least intensity value of the image I .

Hence FS I_A of the image I is defined as

$$I_A = \{ \langle I(i, j), \mu_I(I(i, j)) \rangle | 0 \leq i \leq S - 1, \\ 0 \leq j \leq T - 1, 0 \leq I(i, j) \leq L - 1, \\ 0 \leq \mu_I(I(i, j)) \leq 1 \}.$$

For instance, consider an image C of size 3×3 , whose intensity values are represented in a matrix as follows:

$$C = \begin{bmatrix} 25 & 191 & 25 \\ 191 & 127 & 191 \\ 25 & 191 & 25 \end{bmatrix}$$

Fuzzification is a process of transformation of gray-level range $[0, 255]$ to the interval $[0, 1]$. In this paper fuzzification has been chosen as the normalization of the intensity values, for more details about fuzzification reader can refer [Balasubramaniam and Ananthi \(2014\)](#). Fuzzified matrix I_C of the image C is given below

$$I_C = \begin{bmatrix} \langle 25, 0 \rangle & \langle 191, 1 \rangle & \langle 25, 0 \rangle \\ \langle 191, 1 \rangle & \langle 127, 0.6145 \rangle & \langle 191, 1 \rangle \\ \langle 25, 0 \rangle & \langle 191, 1 \rangle & \langle 25, 0 \rangle \end{bmatrix}$$

Power of FSs mainly depends on the membership function that is being used in it. Even though FSs depend on the membership function, there arises hesitation in defining brightness quantity of the chosen pixel in an image due to poor illumination of brain images. This leads to grayness ambiguity. The main aim of this work is to remove uncertainty in quoting membership values of the pixels of the uncertain brain MR image. Hence fuzzified image is again transformed to an image in intuitionistic fuzzy domain having three parameters. It should be clearly noted that one can select the membership function intuitively. We use IFS to develop IVIFS to remove ambiguity in allocation of membership values to each pixel.

Mostly, intuitionistic fuzzy generators are employed to construct IFS. The degree of membership of IFS is computed as

$$\mu_F(I(i, j)) = 0.582 \left(\exp(1 - |\mu_I(I(i, j)) - m_I|) - 1 \right), \tag{2}$$

where $\mu_I(I(i, j))$ is obtained from Eq. (1) and m_I denotes the mean intensity value of μ_I (constructed using restricted equivalence function).

The degree of non-membership function is defined as

$$\nu_F(I(i, j)) = \frac{1 - \mu_F(I(i, j))}{1 + \lambda \times \mu_F(I(i, j))}, \lambda > 0. \tag{3}$$

For more details about non-membership function, see [Bustince et al. \(2000\)](#). Finally, an IFS is formulated as

$$F = \left\{ \langle I(i, j), \mu_F(I(i, j)), \nu_F(I(i, j)), \pi_F(I(i, j)) \rangle, I(i, j) \in \{0, 1, \dots, L - 1\} \right\},$$

where

$$\pi_F(I(i, j)) = 1 - \mu_F(I(i, j)) - \nu_F(I(i, j)). \tag{4}$$

For illustration, the image C in IFS domain is described as follows, which is obtained using the membership function of the fuzzy image I_C into Eq. (2). Let F_C denote the IFS of the image C with membership function μ_{F_C} , non-membership function ν_{F_C} , and the hesitation degree π_{F_C} . Hence the image in IFS domain is represented as

$$F_C = \left[\begin{array}{ccc} \langle 25, 0.3654, 0.4910, 0.1435 \rangle & \langle 191, 0.3898, 0.4651, 0.1451 \rangle & \langle 25, 0.3654, 0.4910, 0.1435 \rangle \\ \langle 191, 0.3898, 0.4651, 0.1451 \rangle & \langle 127, 0.8470, 0.0912, 0.0618 \rangle & \langle 191, 0.3898, 0.4651, 0.1451 \rangle \\ \langle 25, 0.3654, 0.4910, 0.1435 \rangle & \langle 191, 0.3898, 0.4651, 0.1451 \rangle & \langle 25, 0.3654, 0.4910, 0.1435 \rangle \end{array} \right]$$

3.2 Construction of IVIFS from IFS

Even though the value of membership function is assigned by reducing hesitation in allotting the exact value, still there exists some uncertainty whether the chosen value is appropriate. Hence one can opt a range of values rather than an exact value. For this reason, IVIFS is utilized to remove such vagueness that exist in IFS. IVIFS is constructed as in [Bustince and Burillo \(1995\)](#) by defining a mapping as follows.

Consider the mapping

$$F_C = \left[\begin{array}{ccc} \langle 25, [0.3511, 0.3798], [0.4767, 0.5054] \rangle & \langle 191, [0.3753, 0.4043], [0.4506, 0.4796] \rangle & \langle 25, [0.3511, 0.3798], [0.4767, 0.5054] \rangle \\ \langle 191, [0.3753, 0.4043], [0.4506, 0.4796] \rangle & \langle 127, [0.8408, 0.8532], [0.0850, 0.0974] \rangle & \langle 191, [0.3753, 0.4043], [0.4506, 0.4796] \rangle \\ \langle 25, [0.3511, 0.3798], [0.4767, 0.5054] \rangle & \langle 191, [0.3753, 0.4043], [0.4506, 0.4796] \rangle & \langle 25, [0.3511, 0.3798], [0.4767, 0.5054] \rangle \end{array} \right]$$

$$\phi : \text{IFS}(X) \rightarrow \text{IVIFS}(X)$$

defined as

$$\phi(F) = \{ \langle x, M_{\phi(F)}(x), N_{\phi(F)}(x) \rangle | x \in X \} = \tilde{F},$$

where $M_{\phi(F)}$ and $N_{\phi(F)}$ are split into the following lower and upper intuitionistic fuzzy interval elements.

- (1) $M_{\phi(F)L}(x) = M_{\tilde{F}L}(x) = \mu_F(x) - p \cdot \pi_F(x), \quad 0 \leq p \leq \frac{\mu_F(x)}{\pi_F(x)}$.
- (2) $M_{\phi(F)U}(x) = M_{\tilde{F}U}(x) = \mu_F(x) + \alpha \cdot \pi_F(x), \quad 0 \leq \alpha \leq 1$.
- (3) $N_{\tilde{F}L}(x) = \nu_F(x) - q \cdot \pi_F(x), \quad 0 \leq q \leq \frac{\nu_F(x)}{\pi_F(x)}$.
- (4) $N_{\tilde{F}U}(x) = \nu_F(x) + \beta \cdot \pi_F(x), \quad 0 \leq \beta \leq 1$,
with $0 \leq \alpha + \beta \leq 1, 0 < \alpha + p \leq 1$ and $0 < \beta + q \leq 1$.

Define $W_{M\tilde{F}}(x) = M_{\tilde{F}U}(x) - M_{\tilde{F}L}(x) = (\alpha + p) \cdot \pi_F(x)$ and $W_{N\tilde{F}}(x) = N_{\tilde{F}U}(x) - N_{\tilde{F}L}(x) = (\beta + q) \cdot \pi_F(x)$, then it is clearly seen that IVIFSs are constructed in such a way that the membership and non-membership interval's width does not surmount its intuitionistic fuzzy index (π_F). Suppose if $F \in FSS(X)$, then

$$\phi(F) = \{ \langle x, M_{\phi(F)}(x), N_{\phi(F)}(x) \rangle | x \in X \} \text{ with } \pi_F(x) = 0,$$

which implies

$$M_{\tilde{F}L}(x) = M_{\tilde{F}U}(x) = \mu_F(x)$$

$$N_{\tilde{F}L}(x) = N_{\tilde{F}U}(x) = \nu_F(x)$$

and hence $\phi(F) = F$. Therefore, if $F \in FSS(X)$ then $\phi(F) = F$.

For example, IVIFS \tilde{F}_C of the image C is constructed with the parameters $\alpha = \beta = p = q = 0.1$ using the membership function μ_{F_C} and the hesitation degree π_{F_C} of IFS of the image C and it is presented as follows:

4 Segmentation process

Each and every brain MR slice needs to be pre-processed before segmentation. This section describes the pre-processing first and then depicts the steps of the segmentation

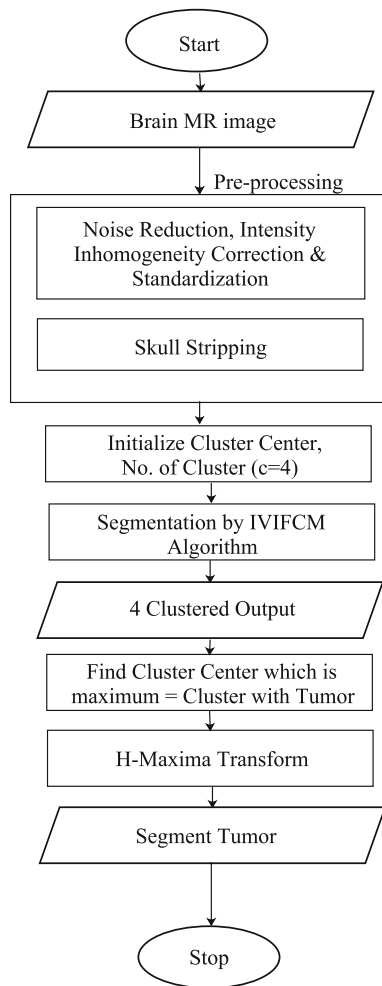


Fig. 1 Flowchart of the proposed algorithm

process. Flow chart of the proposed segmentation process is depicted in Fig. 1.

4.1 Pre-processing

Extraction of brain region is one of the main pre-processing tasks required for the source brain MR image dataset shown in Fig. 2 earlier to the segmentation of tumor.

4.1.1 Filtering to reduce noise

Each brain MR image is filtered to enhance the image quality. Presence of noise in images masks some important characteristics of the MR image and this makes image analysis a difficult task. Here, median filter is used to remove noise. But this filter smooths the image edges, so unsharp masking is done after filtering and is executed using 2D Laplacian, for more detail, see [Gonzalez and Woods \(2008\)](#).

4.1.2 Intensity inhomogeneity correction and standardization

Variation in magnetic field causes non-uniformity in the intensities of the images. There are numerous methods available in literature ([Hou 2006](#); [Wells et al. 1996](#)) to correct intensity inhomogeneity. Standardization is a pre-processing technique that relates nonlinear gray-scale intensity levels of an image into a standard gray-scale intensity levels by training and transformation. This process helps during registration and segmentation. Segmentation algorithm works better when global intensity patterns are related to a certain scale of local patterns ([Zhung and Udupa 2009](#)). Before extracting the brain MR image dataset, intensity of MR slices is standardized by adopting the method which is given in [Nyul and Udupa \(1999\)](#) with $[s_1, s_2] = [0, 255]$.

4.1.3 Brain region extraction

Extraction of the brain portion from brain MR image is an essential part in segmentation. Generally, MR image comprises brain and non-brain regions (skull, fat). Due to high intensity of non-brain parts, misclassification in clustering occurs, see [Roslan et al. \(2011\)](#). Hence it is necessary to remove skull and non-brain tissues from brain MR images by a process of skull stripping. Many algorithms are available in the literature to extract brain region. Brain extraction tool introduced in [Smith \(2002\)](#) is utilized in this paper for the removal of non-brain regions. Extracted brain portions of the source image after standardization and intensity inhomogeneity correction are shown in Fig. 3.

4.2 Clustering brain MR image using IVIFCM algorithm

Basically a MR brain image with tumor is divided into four regions (white matter (WM), gray matter (GM), cerebrospinal fluid (CSF), and abnormal region). The steps of IVIFCM algorithm for segmenting tumor are as follows.

Step 1

Let I be a brain MR image received after pre-processing the given image of size $n (= S \times T)$. Then model the image I in IVIFS domain as illustrated previously. Fix the cluster class $c = 4$, fuzzification index $m > 0$, end limit $\epsilon > 0$, and iteration counter t .

Step 2

Initialize the cluster center $V^{(t)}$ at $t = 0$.

Step 3

For t th iteration, compute the membership matrix U by adopting the following expression:

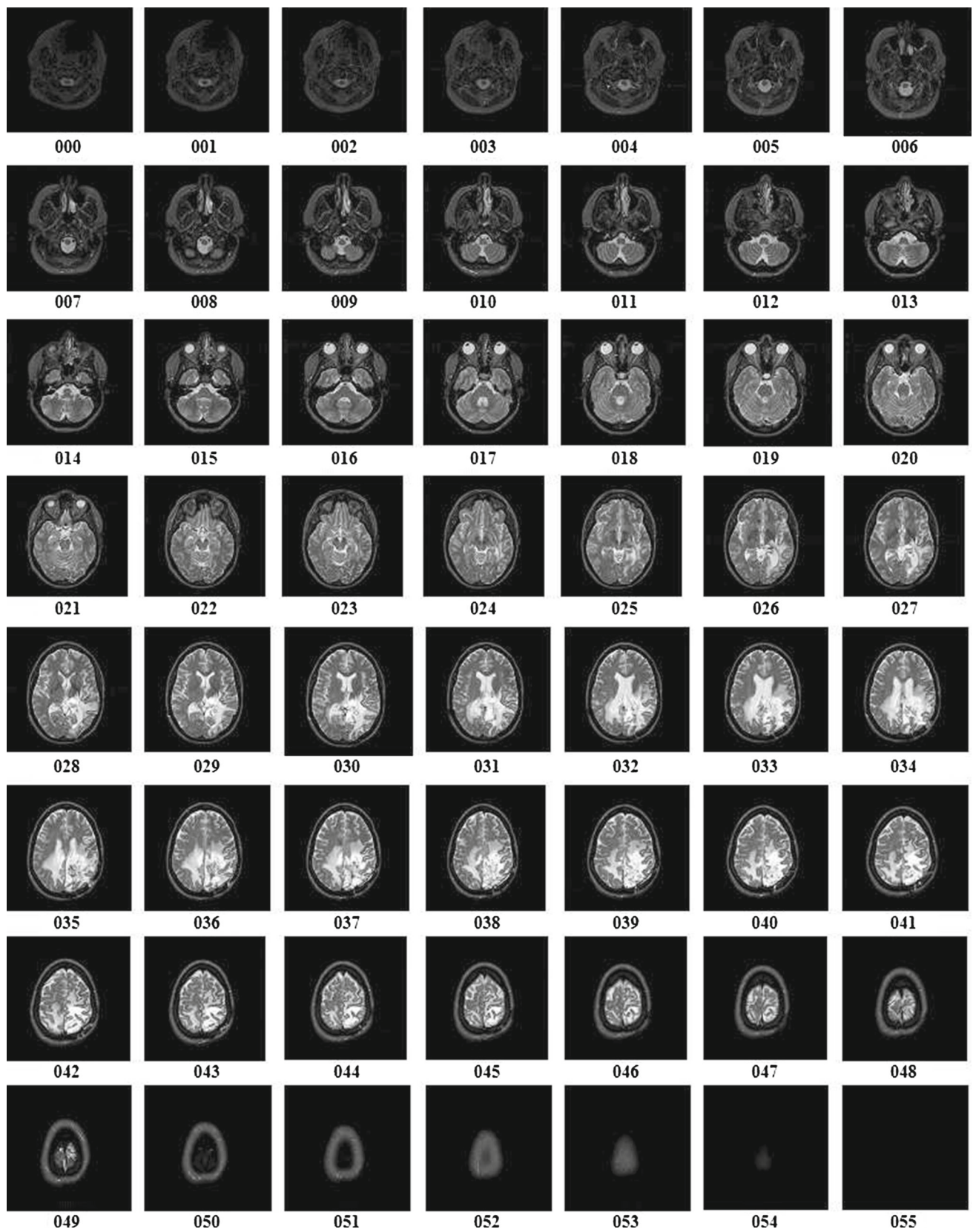


Fig. 2 Source brain MR image dataset

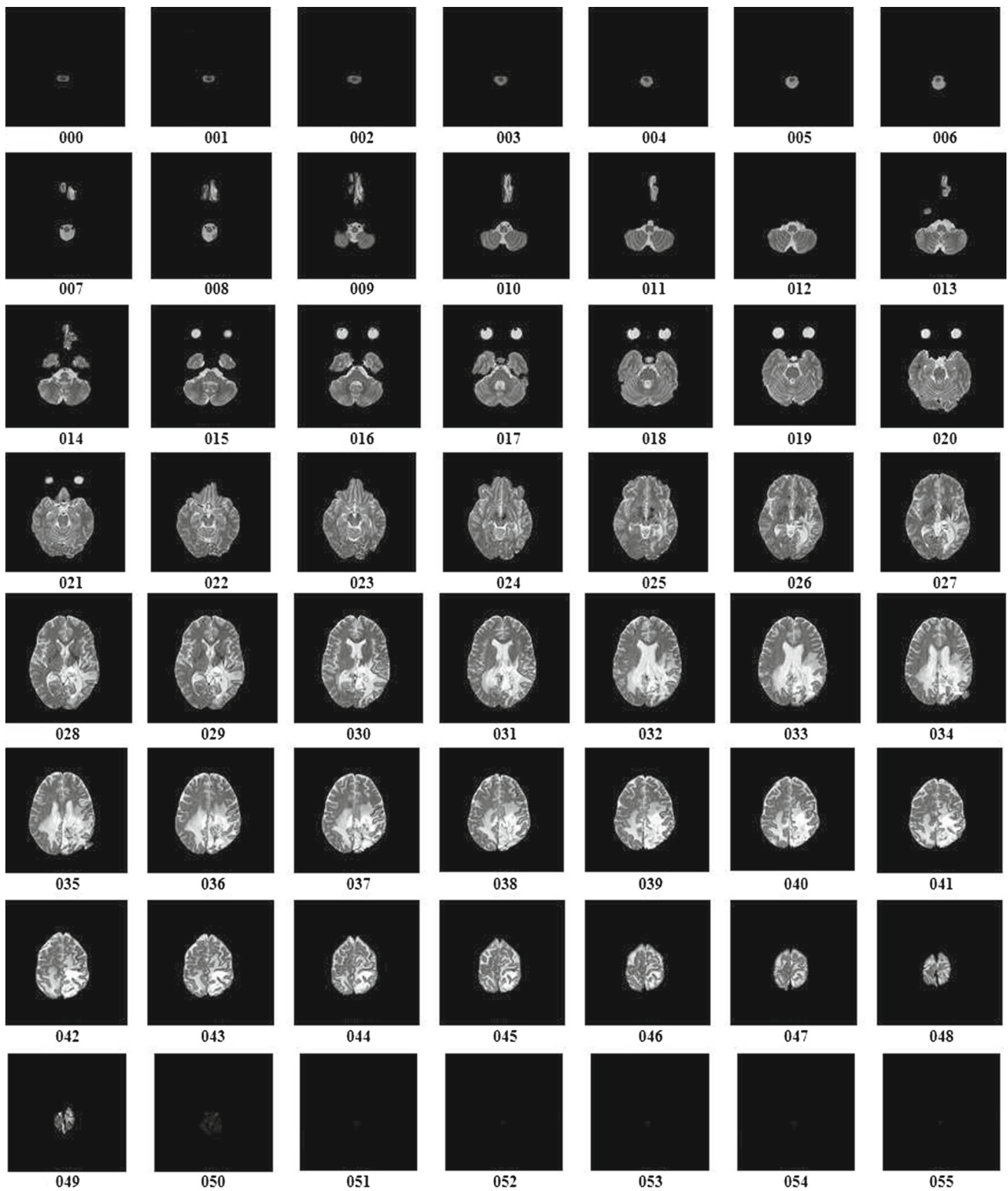


Fig. 3 Pre-processed brain MR image dataset

$$u_{ik}^{(t)} = \begin{cases} \frac{1}{\sum_{i=1}^c \left(\frac{d^{(t)}(x_k, v_i)}{d^{(t)}(x_j, v_i)} \right)^{\frac{2}{m-1}}}, & \text{if } d^{(t)}(x_j, v_i) > 0; \\ 1, & \text{if } d^{(t)}(x_j, v_i) = 0, \end{cases} \quad (5)$$

$$J_m = \sum_{i=1}^c \sum_{k=1}^n (u_{ik}^*)^m d_{ik}^2 + \sum_{i=1}^c W_{M\tilde{F}}^*(x_i) \times e^{1-W_{M\tilde{F}}^*(x_i)}, \quad (8)$$

where $d(x_k, v_i) = \frac{1}{2}\sqrt{\text{dist}}$ with

$$\text{dist} = \sum_{k=1}^n \left\{ [M_{\tilde{F}L}(x_k) - M_{\tilde{F}L}(v_i)]^2 + [M_{\tilde{F}U}(x_k) - M_{\tilde{F}U}(v_i)]^2 + [N_{\tilde{F}L}(x_k) - N_{\tilde{F}L}(v_i)]^2 + [N_{\tilde{F}U}(x_k) - N_{\tilde{F}U}(v_i)]^2 + [W_{M\tilde{F}}(x_k) - W_{M\tilde{F}}(v_i)]^2 + [W_{N\tilde{F}}(x_k) - W_{N\tilde{F}}(v_i)]^2 \right\}$$

Step 4

A new membership matrix U^* is computed for t^{th} iteration using the formula

$$U^* = U^{(t)} + W_{M\tilde{F}}^{(t)}, \quad (6)$$

where $W_{M\tilde{F}}^{(t)}$ is computed as in the Sect. 3.2 by implementing the membership values obtained in step 3 into Eq. (1).

Step 5

Update cluster center $V^{(t+1)}$ by utilizing the following expression:

$$U(0) = \begin{bmatrix} 0.7232 & 0.4324 & 0.7232 & 0.4324 & 0.7497 & 0.4324 & 0.7232 & 0.4324 & 0.7232 \\ 0.6603 & 0.8176 & 0.6603 & 0.8176 & 0.9216 & 0.8176 & 0.6603 & 0.8176 & 0.6603 \\ 0.4430 & 0.5646 & 0.4430 & 0.5646 & 0.8191 & 0.5646 & 0.4430 & 0.5646 & 0.4430 \end{bmatrix}$$

where $W_{M\tilde{F}}^*(x_i) = \frac{1}{n} \sum_{i=1}^n W_{M\tilde{F}}(x_i)$.

The process of IVIFCM clustering algorithm to cluster a 3×3 image C is explained as follows:

Step 1

Let $c = 3$, $m = 2$, and $\epsilon = 0.001$. For a 3×3 image C , $n = 9$. Randomly select initial centroid $V(0)$ from the image. For instance, the centers are considered as

$$V(0) = \begin{bmatrix} 0.9711 \\ 0.9767 \\ 0.9483 \end{bmatrix}$$

Step 2

Calculate the upper and lower membership degrees, non-membership degrees, and the width of the membership and non-membership degrees of the image by generating IVIFS from IFS as defined in the Sect. 3. Using Eq. (5), one can have the extended membership matrix as

Step 3

A new membership matrix is computed according to Eq. (6), we have

$$U^*(0) = \begin{bmatrix} 0.7435 & 0.4615 & 0.7435 & 0.4615 & 0.7685 & 0.4615 & 0.7435 & 0.4615 & 0.7435 \\ 0.6838 & 0.8320 & 0.6838 & 0.8320 & 0.9283 & 0.8320 & 0.6838 & 0.8320 & 0.6838 \\ 0.4721 & 0.5917 & 0.4721 & 0.5917 & 0.8335 & 0.5917 & 0.4721 & 0.5917 & 0.4721 \end{bmatrix}$$

Step 4

Update the centers for $t = 1$ according to equation Eq. (7) as follows:

$$V(1) = \begin{bmatrix} 0.9550 \\ 0.9382 \\ 0.8949 \end{bmatrix}$$

Step 6

If distance between the membership matrix got from the present $(t + 1)$ th and previous (t) th iteration is less than ϵ , then stop the process. Else go to step 3 by fixing t as $t + 1$.

It is observed that the new membership matrices acquired are selected in such a way to minimize the objective function J_m defined as

Step 5

Calculate the membership matrix for $t = 1$ according to equation Eq. (5) by utilizing the centers obtained from step 4 as

$$U^*(1) = \begin{bmatrix} 0.5805 & 0.2939 & 0.5805 & 0.2939 & 0.6300 & 0.2939 & 0.5805 & 0.2939 & 0.5805 \\ 0.5794 & 0.6231 & 0.5794 & 0.6231 & 0.8332 & 0.6231 & 0.5794 & 0.6231 & 0.5794 \\ 0.2556 & 0.5859 & 0.2556 & 0.5859 & 0.7759 & 0.5859 & 0.2556 & 0.5859 & 0.2556 \end{bmatrix}$$

Step 6

Check the distance between membership matrices obtained during iterations there by minimizing the objective function defined in Eq. (8). Let D denote the distance, then we have

$$D(U^*(1), U^*(0)) = 0.0063 > 0.001$$

Since this distance is not small enough, so the iteration is continued as follows:
When $t = 2$

$$V(2) = \begin{bmatrix} 0.9892 \\ 0.8646 \\ 0.8547 \end{bmatrix}$$

$$U^*(2) = \begin{bmatrix} 0.5793 & 0.2672 & 0.5793 & 0.2672 & 0.6510 & 0.2672 & 0.5793 & 0.2672 & 0.5793 \\ 0.5790 & 0.5825 & 0.5790 & 0.5825 & 0.3237 & 0.5825 & 0.5790 & 0.5825 & 0.5790 \\ 0.2544 & 0.5923 & 0.2544 & 0.5923 & 0.5958 & 0.5923 & 0.2544 & 0.5923 & 0.2544 \end{bmatrix}$$

$$D(U^*(2), U^*(1)) = 0.0051 > 0.001$$

Since this distance is not small enough, so the iteration is continued when $t = 3$

$$V(3) = \begin{bmatrix} 0.9892 \\ 0.8646 \\ 0.8547 \end{bmatrix}$$

$$U^*(3) = \begin{bmatrix} 0.5790 & 0.2542 & 0.5790 & 0.2542 & 0.5790 & 0.2542 & 0.5790 & 0.2542 & 0.5790 \\ 0.5790 & 0.5790 & 0.5790 & 0.5790 & 0.2542 & 0.5790 & 0.5790 & 0.5790 & 0.5790 \\ 0.2542 & 0.5790 & 0.2542 & 0.5790 & 0.5790 & 0.5790 & 0.2542 & 0.5790 & 0.2542 \end{bmatrix}$$

$$D(U^*(3), U^*(2)) = 0.0001 < 0.001$$

Hence one can stop the iterations. Then defuzzification is applied by inverting the fuzzification process. The new defuzzified membership matrix is given by

$$U = \begin{bmatrix} 0 & 0.9389 & 0 & 0.9389 & 0 & 0.9389 & 0 & 0.9389 & 0 \\ 0 & 0 & 0 & 0 & 0.9389 & 0 & 0 & 0 & 0 \\ 0.9389 & 0 & 0.9389 & 0 & 0 & 0 & 0.9389 & 0 & 0.9389 \end{bmatrix}$$

If we assume that $u_{ij} \geq 0.75$, the clustered result of the image C is shown in the Table 1.

Table 1 Clustering result of the image C by IVIFCM

Image pixels	Cluster ID
$c_{12}, c_{21}, c_{23}, c_{32}$	1
c_{22}	2
$c_{11}, c_{13}, c_{31}, c_{33}$	3

4.3 Separation of tumor region from appropriate cluster

From the four clustered output, cluster center with tumor region is determined by choosing cluster center with maxi-

imum value. Let us discuss about why one should select an image with maximum cluster center and whether this hap-

pens for all the cases of images? T1-weighted, T2-weighted, and proton density-weighted images are the three main types of MR images. For example, in T2-weighted MR slices, WM

appears as dark gray, GM as gray, and CSF and tumor cells appear as bright pixels. Hence one can consider a cluster

which is having maximum cluster center that corresponds to bright pixels in the image and this region represents the CSF and the tumor. Then it is necessary to separate tumor from the CSF, for such purpose H-max transformation has been applied. The tumor region will have brightest pixel value in T2-weighted MR images, but this does not happen in the case of T1-weighted MR images. For such cases, contrast-enhanced brain MR images can be utilized for clustering. In the contrast-enhanced images tumor regions have enough brightness, so in this case also one can find the clustered image with tumor by searching a cluster with maximum cluster center. After choosing an appropriate cluster, it is necessary to segment exact tumor region. For this, maxima transform is used to find tumor position. H-maxima transform Soille (1999) determines the peaks having h intensity rates greater than the background in that region. It is robust but highly relies on contrast.

H-maxima transform for an image is generated using morphological operations such as iterated dilations of an image and later it is masked. Koh et al. (2009) have defined H-maxima transform as

$$H_{\max_h}(I) = R_I(I - h),$$

where $R_I(I - h)$ is the retraced image by dilating I with respect to $I - h$. This inhibits all pixels whose intensity rate is lesser than the threshold when the value is compared to their neighbors. Then find all regional maximum of image and separate the pixels of constant intensity. Maxima operation is carried out using the equation

$$T_{\max_h}(I) = R_{\max}(H_{\max_h}(I)) \quad (9)$$

Regional maxima of H-maxima transformed cluster image having tumor is used to eliminate local pixels of intensity less than h from the background. Using Eq. (9), final exact tumor region is extracted without edema and other non-tumor region. For the brain MR slice numbered 040, the clustered image with tumor and the extracted tumor region using H-maxima transform are shown in Fig. 4.

5 Qualitative metrics

Evaluation metrics are used to access the performance of segmentation algorithm (Sokolova and Lapalme 2009) and one of the commonly used metrics is Dice coefficient. Various performance metrics are also available in literature.

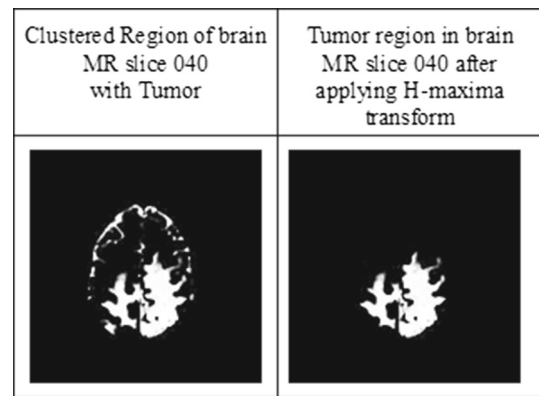


Fig. 4 H-maxima transformation of the brain MR slice 040

5.1 Dice coefficient

Dice similarity coefficient is used to show the similarity level of extracted tumor region with respect to the manually segmented tumor region. It is mathematically formulated as

$$\text{Dice} = \frac{2|A \cap B|}{|A| + |B|},$$

where A is manually segmented tumor region and B is the extracted tumor region obtained using the proposed method. If the Dice coefficient value is 1, then it shows the perfect overlap between A and B . Else if its value is 0, then there is no overlap between A and B .

5.2 Precision

It computes the percentage of positive prediction made by the classifier that are correct.

$$\text{Precision} = \frac{\text{tp}}{\text{tp} + \text{fp}},$$

where true positive (tp) is the number of positive classes correctly classified as positive and false positive (fp) is the number of positive classes incorrectly classified as positive.

5.3 Recall

It computes the percentage of positive patterns that are correctly detected by the classifier.

$$\text{Recall} = \frac{\text{tp}}{\text{tp} + \text{fn}},$$

where true positive (tp) is the number of positive classes correctly classified as positive and false negative (fn) is the number of positive classes incorrectly classified as negative.

Fig. 5 Segmented results of brain MR slices from 023 to 035

Brain tumor data set 4	Segmented Output						
	Manual	IVIFCM	HT	KM	FCM	IFCM	ITFCM
023							
024							
025							
026							
027							
028							
029							
030							
031							
032							
033							
034							
035							



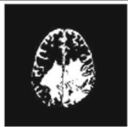







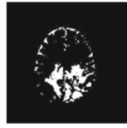

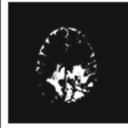




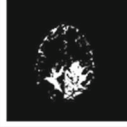





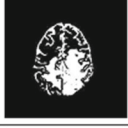
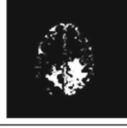

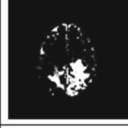

















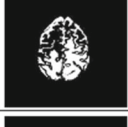



































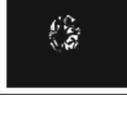
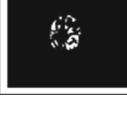


Brain tumor data set 4	Segmented Output						
	Manual	IVIFCM	HT	KM	FCM	IFCM	ITFCM
036							
037							
038							
039							
040							
041							
042							
043							
044							
045							
046							
047							

Fig. 6 Segmented results of brain MR slices from 036 to 047

Table 2 Dice coefficient

Brain MR slice	HT	KM	FCM	IFCM	ITFCM	IVIFCM
023	0.8624	0.9205	0.9280	0.9795	0.9621	0.9957
024	0.8522	0.9064	0.9104	0.9709	0.9705	0.9871
025	0.8408	0.8959	0.8948	0.9486	0.9478	0.9661
026	0.8428	0.8915	0.8930	0.9383	0.9377	0.9548
027	0.8387	0.8727	0.8717	0.9242	0.9266	0.9420
028	0.8361	0.8701	0.8685	0.9268	0.9317	0.9415
029	0.8225	0.8731	0.8674	0.9280	0.9301	0.9432
030	0.8167	0.8876	0.8820	0.9319	0.9344	0.9478
031	0.8156	0.8747	0.8727	0.9174	0.9193	0.9344
032	0.8107	0.8713	0.8731	0.9199	0.9231	0.9478
033	0.8118	0.8678	0.8678	0.9117	0.9134	0.9330
034	0.8160	0.8774	0.8714	0.9168	0.9185	0.9326
035	0.8240	0.8785	0.8703	0.9194	0.9210	0.9298
036	0.8332	0.8877	0.8819	0.9301	0.9315	0.9364
037	0.8238	0.8838	0.8733	0.9259	0.9286	0.9335
038	0.8245	0.8770	0.8767	0.9212	0.9229	0.9231
039	0.8419	0.8978	0.8980	0.9389	0.9418	0.9450
040	0.8523	0.8991	0.8941	0.9391	0.9413	0.9451
041	0.8605	0.9030	0.8968	0.9368	0.9403	0.9440
042	0.8669	0.9065	0.9046	0.9364	0.9381	0.9438
043	0.8807	0.9203	0.9288	0.9568	0.9568	0.9621
044	0.8974	0.9324	0.9366	0.9562	0.9573	0.9605
045	0.9072	0.9271	0.9309	0.9480	0.9482	0.9551
046	0.9304	0.9474	0.9432	0.9665	0.9370	0.9758
047	0.9473	0.9621	0.9574	0.9780	0.9760	0.9872

5.4 Precision–recall and ROC curves

Precision–recall curves show the relationship among precision and recall as segmentation threshold varies.

The receiver operating characteristic (ROC) is a graph, which renders the relationship between true-positive rate (TPR) and false-positive rate (FPR) as there is a variation in threshold. For a classifier, it depicts that TPR cannot increase without an increasing FPR.

$$\text{TPR} = \text{Recall}$$

$$\text{FPR} = \frac{\text{fp}}{\text{Total negative}}$$

5.5 Area of tumor

The dimension of each slice in the datasets is 256×256 pixels and slice thickness is 5 with 260 mm field of view. Therefore, the pixel dimension is fixed to $1 \text{ mm} \times 1 \text{ mm}$.

Area of one pixel $A = H \times V$, where H and V represent the horizontal and vertical dimension of the pixel $= 1 \text{ mm} \times 1 \text{ mm} = 1 \text{ mm}^2$.

Area of tumor region in the 2D slice = $A \times$ Number of (white) pixels in the segmented output image.

6 Experimental results and discussions

The datasets for experimental analysis were obtained from KGS Advanced MR and CT Scan, Madurai, Tamil Nadu, India. Tests are executed on numerous brain MR image datasets having tumor. Among them, only one dataset with 55 slices (given in Fig. 2) is presented in this paper to show the performance of the proposed algorithm. After noise removal, intensity inhomogeneity correction, and standardization of intensities in the brain MR image dataset, the dataset is fed into brain extraction process for removing non-brain regions. Skull-stripped brain MR image dataset obtained after pre-processing has shown in Fig. 3. Skull-stripped brain MR image data are then fed into the clustering process by fixing the cluster center c as 4.

For each slice four clustered outputs are obtained. In order to find a cluster which is having tumor, find a cluster class with maximum cluster center when compared to other three cluster classes and that cluster class is consid-

Table 3 Tumor area

Brain MR slice	HT $\times 10^{-3} \text{ m}^2$	KM $\times 10^{-3} \text{ m}^2$	FCM $\times 10^{-3} \text{ m}^2$	IFCM $\times 10^{-3} \text{ m}^2$	ITFCM $\times 10^{-3} \text{ m}^2$	IVIFCM $\times 10^{-3} \text{ m}^2$
023	0.0011	0.1365	0.0776	0.0137	0.0250	0.0012
024	0.0047	0.1460	0.0919	0.0165	0.0157	0.0041
025	0.0112	0.1526	0.0970	0.0228	0.0229	0.0112
026	0.0294	0.1616	0.0897	0.0280	0.0300	0.0284
027	0.0385	0.1656	0.1021	0.0316	0.0301	0.0372
028	0.0437	0.1776	0.1080	0.0358	0.0304	0.0423
029	0.0353	0.1773	0.1076	0.0343	0.0342	0.0352
030	0.0364	0.1866	0.1152	0.0468	0.0424	0.0353
031	0.0362	0.1879	0.1206	0.0544	0.0504	0.0356
032	0.0307	0.1954	0.1277	0.0666	0.0621	0.0314
033	0.0537	0.1992	0.1311	0.0675	0.0504	0.0528
034	0.0502	0.1981	0.1209	0.0600	0.0559	0.0486
035	0.0533	0.1901	0.1202	0.0544	0.0552	0.0532
036	0.0539	0.1825	0.1137	0.0493	0.0462	0.0510
037	0.0522	0.1856	0.1109	0.0410	0.0423	0.0504
038	0.0497	0.1804	0.1089	0.0394	0.0391	0.0494
039	0.0449	0.1684	0.0979	0.0389	0.0385	0.0431
040	0.0462	0.1593	0.0943	0.0383	0.0323	0.0446
041	0.0433	0.1452	0.0859	0.0334	0.0280	0.0413
042	0.0354	0.1328	0.0759	0.0274	0.0283	0.0361
043	0.0233	0.1186	0.0717	0.0168	0.0220	0.0213
044	0.0200	0.0990	0.0577	0.0128	0.0112	0.0208
045	0.0235	0.0873	0.0542	0.0106	0.0110	0.0234
046	0.0119	0.0658	0.0434	0.0159	0.0334	0.0119
047	0.0058	0.0508	0.0341	0.0134	0.0145	0.0063

ered as a clustered tumor region in brain MR slice. Now H-maxima transformation is applied to the resulting brain MR slices with tumor for the extraction of tumor region. Brain MR slices numbered from 023 to 047 in the given source brain MR dataset are found to be having tumor and are operated by H-maxima transformation. Figure 4 is drawn to show how H-maxima transformation separates the tumor from the clustered brain MR slices. The result of this transformation mechanism is shown only for a single brain MR slice numbered 040 and likewise this is done to rest of the slices.

Figures 5 and 6 show the segmented results of the brain MR slices with tumor obtained by various methods such as HT Natarajan et al. (2012), KM Juang and Wu (2010), FCM Chuang et al. (2006), IFCM Chaira (2011), ITFCM Hwang and Rhee (2007), and the proposed IVIFCM method. First column of Figs. 5 and 6 shows the numbers of brain MR slices which have tumor. The results of manually segmented source brain MR slices are shown in the second column of Figs. 5 and 6. Third column of Figs. 5 and 6 portrays the segmented tumor regions using the proposed IVIFCM method

from the brain MR slices with tumor. Fourth column of Figs. 5 and 6 depicts the segmented output obtained using HT. Brain MR slices with tumor are segmented using KM algorithm and are picturized in fifth column of Figs. 5 and 6. One has to note that KM method takes much time for clustering process than other five methods and also the resulting images are over segmented when compared to manually segmented tumor region. Sixth column of Figs. 5 and 6 shows the segmented output obtained using FCM algorithm. From the results obtained using FCM algorithm, it seems to be better than HT and KM method of segmentation. Similarly, brain MR slices with tumor in the given dataset are clustered. Tumor regions are extracted using IFCM and ITFCM algorithms which are depicted in seventh and eighth column of Figs. 5 and 6, respectively.

Dice coefficient of the segmented results of the tumorous brain MR slices is calculated with respect to their manually segmented brain MR slices to show the accuracy of the segmentation process of various methods and whose values are given in Table 2. First column of Table 2 shows the slice numbers which is having tumor in the given dataset. Second

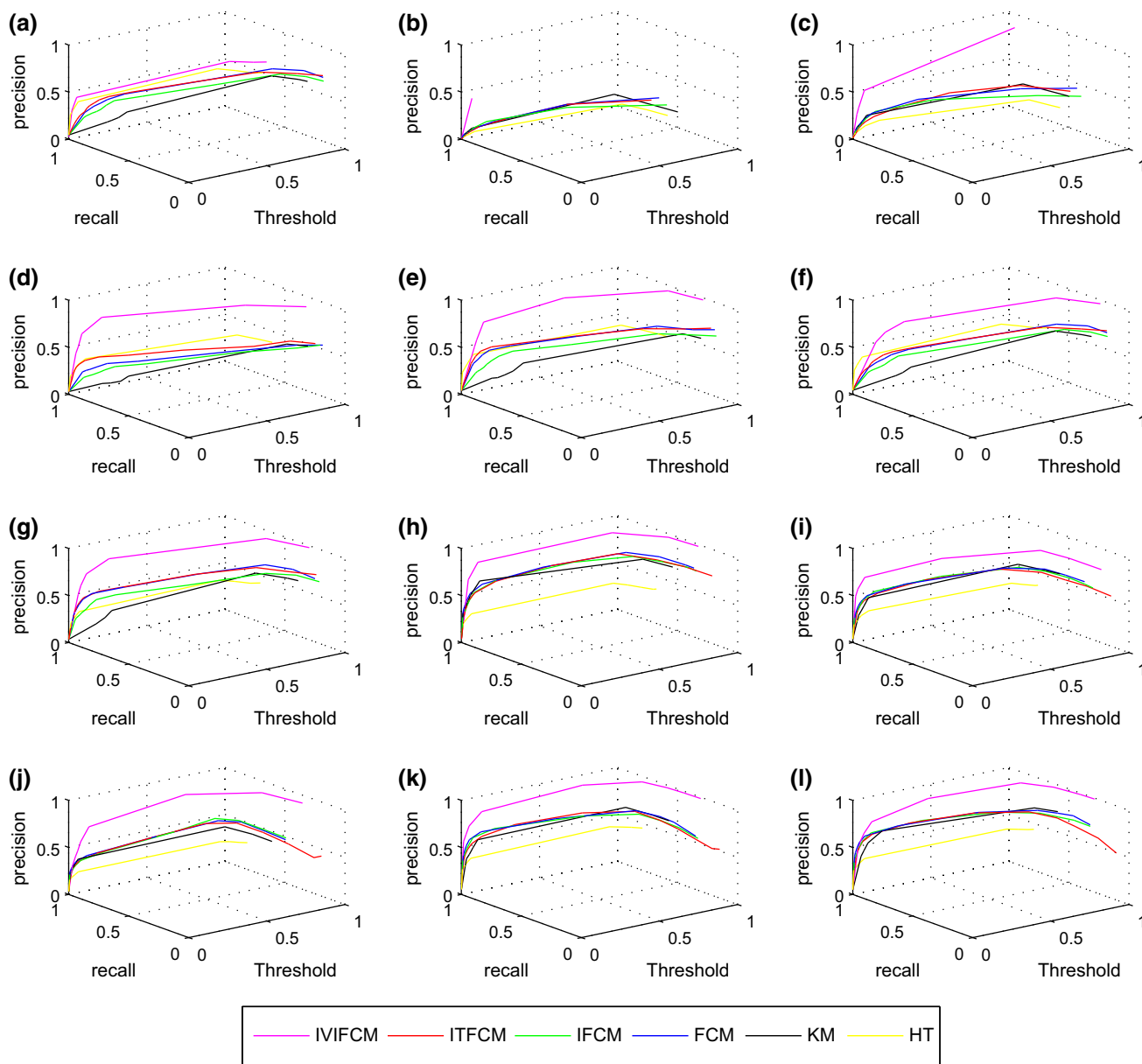


Fig. 7 Precision–recall graphs of brain MR slices from 023 to 034. **a** Precision–recall graph of brain MR slice 023. **b** Precision–recall graph of brain MR slice 024. **c** Precision–recall graph of brain MR slice 025. **d** Precision–recall graph of brain MR slice 026. **e** Precision–recall graph of brain MR slice 027. **f** Precision–recall graph of brain MR slice 028. **g**

Precision–recall graph of brain MR slice 029. **h** Precision–recall graph of brain MR slice 030. **i** Precision–recall graph of brain MR slice 031. **j** Precision–recall graph of brain MR slice 032. **k** Precision–recall graph of brain MR slice 033. **l** Precision–recall graph of brain MR slice 034

to seventh columns of Table 2 show the values of Dice coefficient of the segmented image obtained by HT, KM, FCM, IFCM, ITFCM, and the proposed IVIFCM method, respectively. It is clearly seen that the values of Dice coefficient obtained by the proposed method are high (quoted in bold font) when compared to other five existing methods.

Tumor area of the segmented brain MR slices is computed. Their areas are given in Table 3 for all the segmented outputs obtained manually along with the other five methods and the

proposed method. The best area which is nearer to the area of the tumor obtained through manual segmentation is casted in bold font. Also table shows that the proposed method is the best to find out the tumor region exactly and automatically than the other five existing methods. Tables 2 and 3 quantitatively show that the proposed IVIFCM algorithm is better than other existing methods.

Precision–Recall graphs for the tumorous brain MR slices numbered from 023 to 034 and from 035 to 047 in the given

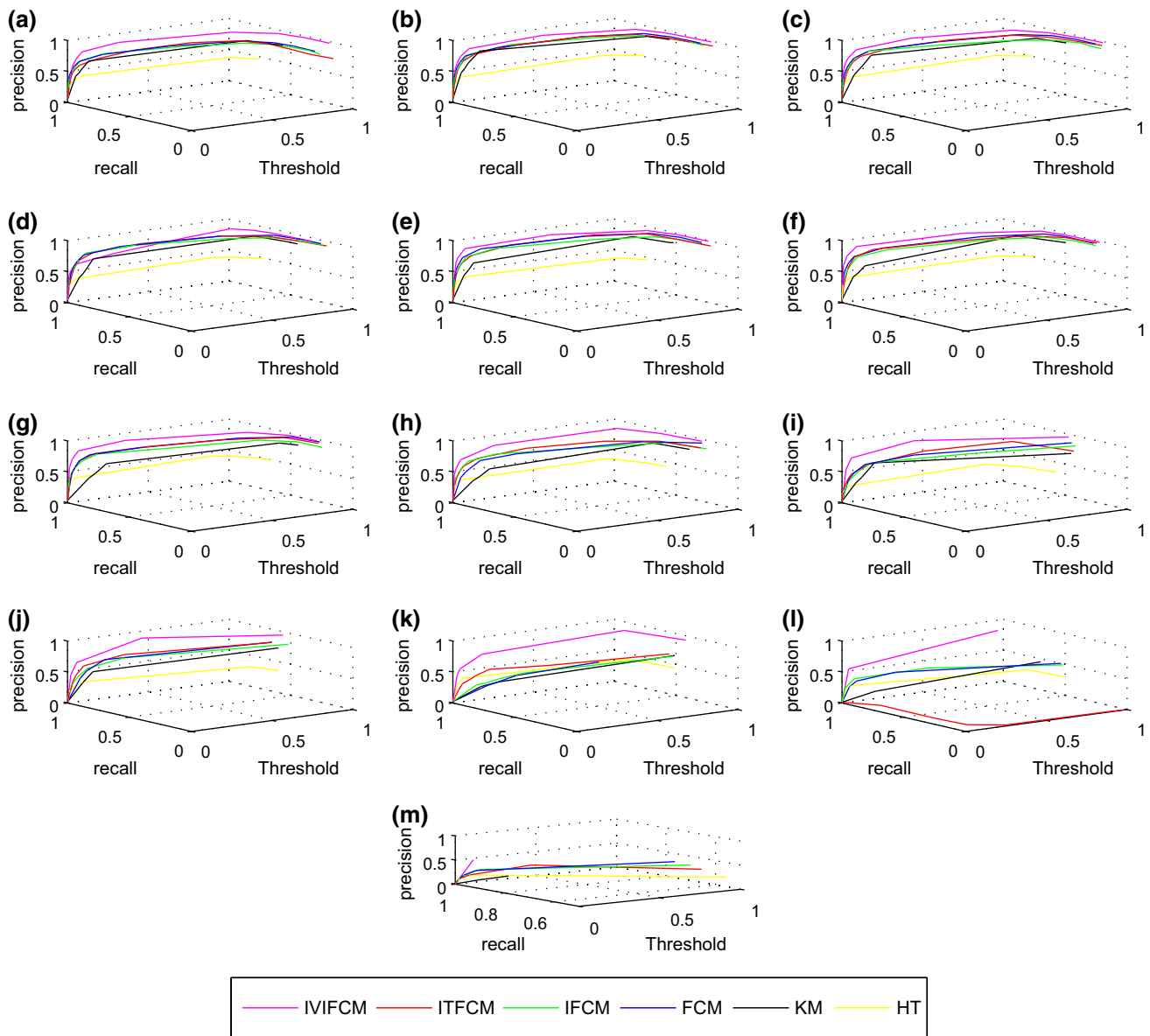


Fig. 8 Precision–recall graphs of brain MR slices from 035 to 047. **a** Precision–recall graph of brain MR slice 035. **b** Precision–recall graph of brain MR slice 036. **c** Precision–recall graph of brain MR slice 037. **d** Precision–recall graph of brain MR slice 038. **e** Precision–recall graph of brain MR slice 039. **f** Precision–recall graph of brain MR slice 040. **g**

Precision–recall graph of brain MR slice 041. **h** Precision–recall graph of brain MR slice 042. **i** Precision–recall graph of brain MR slice 043. **j** Precision–recall graph of brain MR slice 044. **k** Precision–recall graph of brain MR slice 045. **l** Precision–recall graph of brain MR slice 046. **m** Precision–recall graph of brain MR slice 047

dataset are picturized in Figs. 7a–l and 8a–m, respectively. ROC curves of the brain MR slices numbered from 023 to 034 and from 035 to 047 are shown in Figs. 9a–l and 10a–m, respectively. The Precision–Recall and ROC curves vividly describe the effectiveness of the proposed method in all aspects than all other five existing methods.

The proposed clustering method is not only tested on brain MR image slices with tumor but it is also tested on normal brain MR image for checking efficiency of clustering, which

contains three regions namely white matter, gray matter, and cerebrospinal fluid. Precision–Recall and ROC graphs of segmented white matter, gray matter, and cerebrospinal fluid by five various methods are shown in the Fig. 11. Both graphs show that IVIFCM algorithm classifies brain region efficiently than other existing methods. Average dice coefficient for 30 normal brain MR slices is shown in Fig. 12, which also clearly portrays the performance of the proposed clustering algorithm.

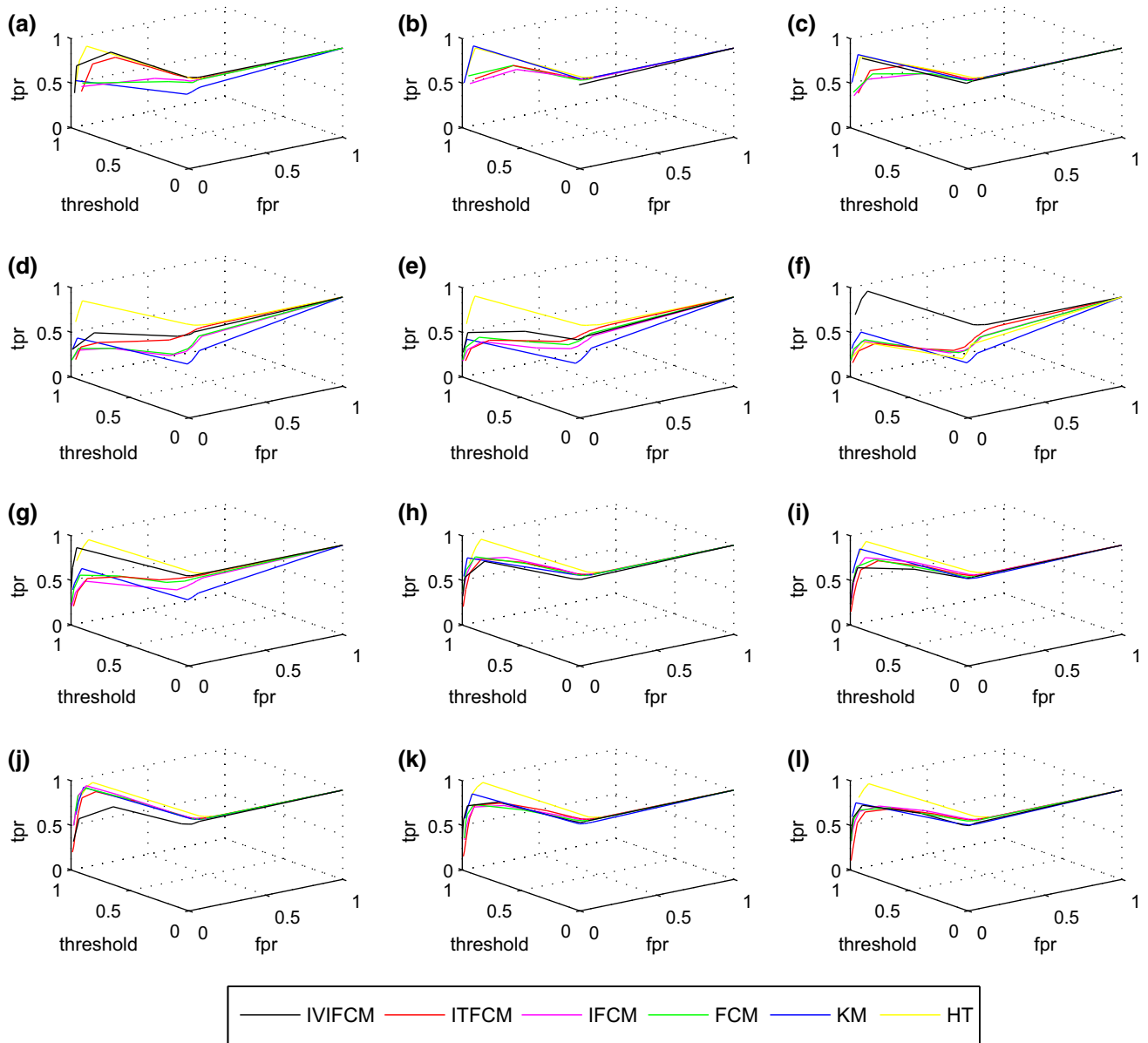


Fig. 9 ROC curves of brain MR slices from 023 to 034. **a** ROC curve of brain MR slice 023. **b** ROC curve of brain MR slice 024. **c** ROC curve of brain MR slice 025. **d** ROC curve of brain MR slice 026. **e** ROC curve of brain MR slice 027. **f** ROC curve of brain MR slice 028.

g ROC curve of brain MR slice 029. **h** ROC curve of brain MR slice 030. **i** ROC curve of brain MR slice 031. **j** ROC curve of brain MR slice 032. **k** ROC curve of brain MR slice 033. **l** ROC curve of brain MR slice 034

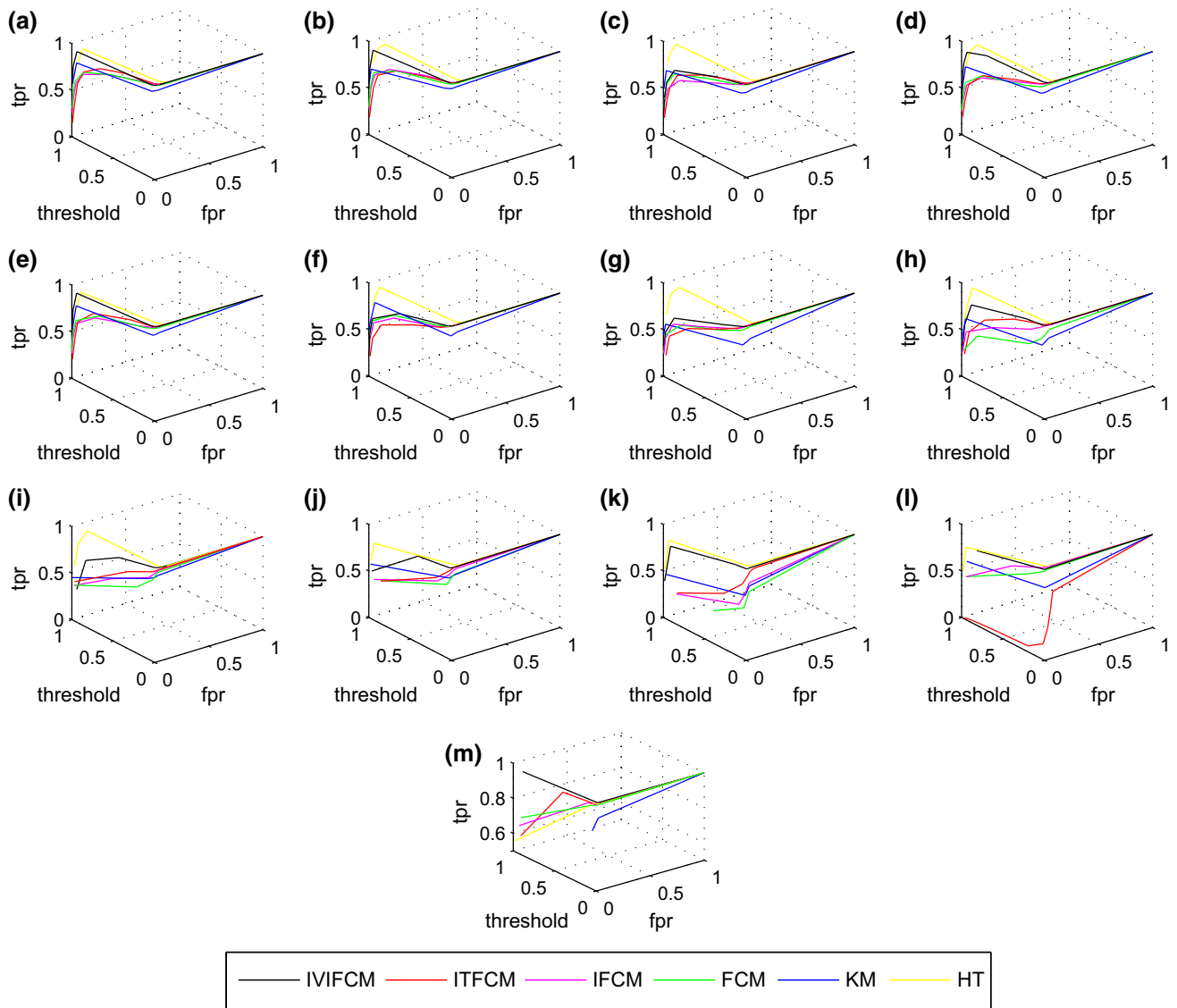


Fig. 10 ROC curves of brain MR slices from 035 to 047. **a** ROC curve of brain MR slice 035. **b** ROC curve of brain MR slice 036. **c** ROC curve of brain MR slice 037. **d** ROC curve of brain MR slice 038. **e** ROC curve of brain MR slice 039. **f** ROC curve of brain MR slice 040.

g ROC curve of brain MR slice 041. **h** ROC curve of brain MR slice 042. **i** ROC curve of brain MR slice 043. **j** ROC curve of brain MR slice 044. **k** ROC curve of brain MR slice 045. **l** ROC curve of brain MR slice 046. **m** ROC curve of brain MR slice 047

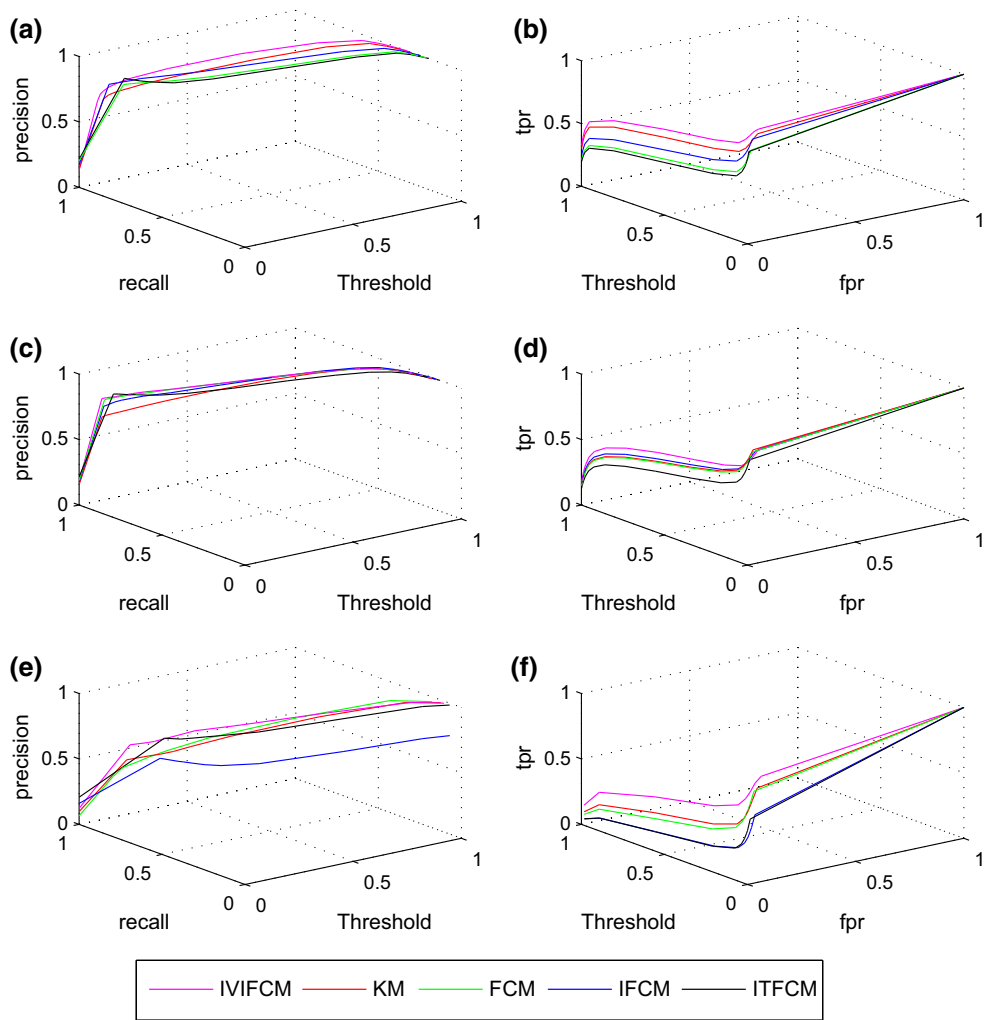


Fig. 11 Precision–recall and ROC curves of normal brain MR image. **a** Precision-recall graph of segmented white matter. **b** ROC curve of segmented white matter. **c** Precision-recall graph of segmented gray

matter. **d** ROC curve of segmented gray matter. **e** Precision-recall graph of segmented CSF. **f** ROC curve of segmented CSF

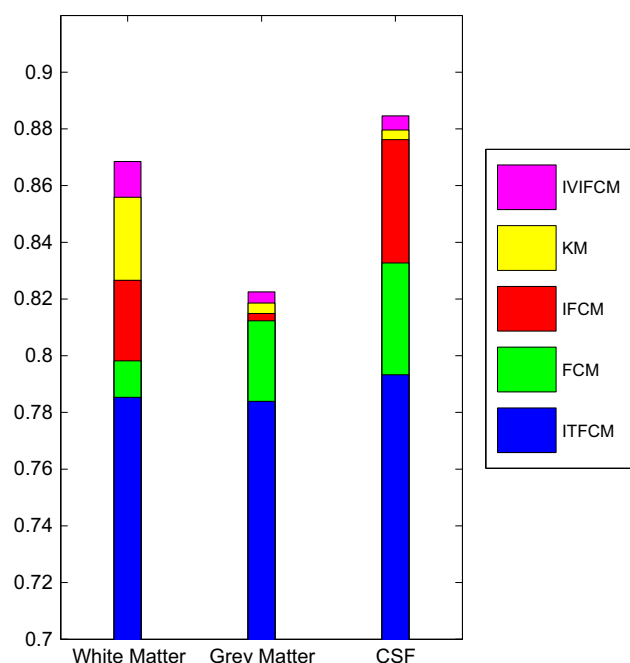


Fig. 12 Average dice coefficient of 30 normal brain MR images

7 Conclusion

A new c-means clustering algorithm has been presented to deal the problem of choosing the values of membership function to symbolize imprecise data with application to medical field. From the proposed method one can choose the value of membership function as an interval instead of a single value, which has obtained using IVIFSs constructed from IFSs. Then IVIFSs generated from the brain MR slices of the given dataset have been clustered by the proposed IVIFCM algorithm. Then tumor region in the clustered output has been found exactly using H-maxima transform. Experimental results have been provided to prove that the proposed algorithm is better than other existing algorithms and tables quantitatively reveal the efficiency of the proposed method.

Acknowledgments This work was supported by UGC-BSR-Research fellowship in Mathematical Sciences—2013–2014. The authors wish to thank all the reviewers and associate editor for their fruitful comments and suggestions for significant improvement of the manuscript.

References

- Agrawal S, Panda R, Dora L (2014) A study on fuzzy clustering for magnetic resonance brain image segmentation using soft computing approaches. *Appl Soft Comput* 24:522–533
- Atanassov KT (1986) Intuitionistic fuzzy sets. *Fuzzy Set Syst* 20:87–96
- Atanassov K, Gargov G (1989) Interval valued intuitionistic fuzzy sets. *Fuzzy Set Syst* 31:343–349
- Balasubramaniam P, Ananthi VP (2014) Image fusion using intuitionistic fuzzy sets. *Inf Fusion* 20:2130
- Bustince H, Kacprzyk J, Mohedano Z (2000) Intuitionistic fuzzy generators application to intuitionistic fuzzy complement. *Fuzzy Set Syst* 114:485–504
- Bustince H, Barrenechea E, Pagola M, Fernandez J (2009) Interval-valued fuzzy sets constructed from matrices: application to edge detection. *Fuzzy Set Syst* 160:1819–1840
- Bustince H, Burillo P (1995) A theorem for constructing interval-valued intuitionistic fuzzy sets from intuitionistic fuzzy sets. *Note Intuit Fuzzy Set* 1:5–16
- Chaira T (2011) A novel intuitionistic fuzzy C-means clustering algorithm and its application to medical images. *Appl Soft Comput* 11:1711–1717
- Chaira T (2014) Accurate segmentation of leukocyte in blood cell images using Atanassovs intuitionistic fuzzy and interval Type II fuzzy set theory. *Micron* 61:1–8
- Chuang KS, Tzeng AL, Chen S, Wu J, Chen TJ (2006) Fuzzy c-means clustering with spatial information for image segmentation. *Comput Med Imaging Graph* 30:9–15
- Farias G, Santos M, Lopez V (2010) Making decisions on brain tumor diagnosis by soft computing techniques. *Soft Comput* 14:1287–1296
- Galdames FJ, Jaillet F, Perez CA (2012) An accurate skull stripping method based on simplex meshes and histogram analysis for magnetic resonance images. *J Neurosci Method* 206:103–119
- Gonzalez RC, Woods RE (2008) Digital image processing, 3rd edn. Prentice Hall, Pearson Education
- Hou Z (2006) A review on MR image intensity inhomogeneity correction. *Int J Biomed Imaging*, pp 1–11. doi:10.1155/IJBI/2006/49515
- Huang CW, Lin KP, Wu MC, Hung KC, Liu GS, Jen CH (2015) Intuitionistic fuzzy c-means clustering algorithm with neighborhood attraction in segmenting medical image. *Soft Comput* 19:459–470
- Hwang C, Rhee FC (2007) Uncertainty fuzzy clustering: interval type-2 fuzzy approach to c-means. *IEEE Trans Fuzzy Syst* 15:107–120
- Ji Z, Xia Y, Sun Q, Cao G (2014) Interval-valued possibilistic fuzzy C-means clustering algorithm. *Fuzzy Set Syst* 253:138–156
- Juang LH, Wu MN (2010) MRI brain lesion image detection based on color-converted k-means clustering segmentation. *Measurement* 43:941–949
- Koh KH, Shen WA, Shuter B, Kassim AA (2009) Segmentation of kidney cortex in MRI studies: a constrained morphological 3D h-maxima transform approach. *Intern J Med Eng Inf* 1:330–341
- Li Y, Shen Y (2010) An automatic fuzzy c-means algorithm for image segmentation. *Soft Comput* 14:123–128
- Natarajan P, Krishnan N, Kenkre NS, Nancy S, Singh BP (2012) Tumor detection using threshold operation in MR brain images. *IEEE Int Conf Comput Intell Comput Res*, pp 1–4
- Nyul LG, Udupa JK (1999) On standardizing the MR image intensity scale. *Magn Reson Med* 42:1072–1081
- Roslan R, Jamil N, Mahmud R (2011) Skull stripping magnetic resonance images brain images: region growing versus mathematical morphology. *Int J Comput Int Syst Ind Manag Appl* 3:150–158
- Smith S (2002) Fast robust automated brain extraction. *Hum Brain Mapp* 17:143–155
- Soille P (1999) Morphological image analysis: principles and applications, 2nd edn. Springer, New York
- Sokolova M, Lapalme G (2009) A systematic analysis of performance measures for classification tasks. *Inf Process Manag* 45:427–437
- Wells WM, Grimson WEL, Kikinis R, Jolesz FA (1996) Adaptive segmentation of MRI data. *IEEE Trans Med Imaging* 15:429–442
- Xu Z, Wu J (2010) Intuitionistic fuzzy c-means clustering algorithms. *J Syst Eng Electron* 21:580–590
- Zadeh LA (1965) Fuzzy sets. *Inf Control* 8:338–353
- Zhao F, Jiao L, Liu H (2013) Kernel generalized fuzzy c-means clustering with spatial information for image segmentation. *Digit Signal Process.* 23:184–199

Zhou D, Zhou H (2014) A modified strategy of fuzzy clustering algorithm for image segmentation. *Soft Comput*, pp 1–12. doi:[10.1007/s00500-014-1481-8](https://doi.org/10.1007/s00500-014-1481-8)

Zhung Y, Udupa JK (2009) Intensity standardization simplifies brain MR image segmentation. *Comput Vis Image Underst* 113:1095–1103